Towards advanced divertor configurations on the J-TEXT tokamak

Yunfeng Liang[1,2,3,*], Zhipeng Chen[1], Nengchao Wang[1], Zhifeng Cheng[1], Alexander Knieps[2], Song Zhou[1], Bo Rao[1], Shuai Xu[2], Philipp Drews[2], Xiaolong Zhang[4], Hao Wang[1], Zhaosu Wang[1], Jie Yang[1,2], Xin Xu[1], Jiankun Hua[1,2], Qinghu Yang[1], Wei Yan[1], Cunkai Li[1], Yutong Yang[1], Shuhao Li[1], Shaocheng Liu[3], Lin Nie[4], Ting Long[4], Liang Liao[2,3], Fuqiong Wang[5], Yasuhiro Suzuki[1,6] and the J-TEXT team

[1] *International Joint Research Laboratory of Magnetic Confinement Fusion and Plasma Physics, State Key Laboratory of Advanced Electromagnetic Engineering and Technology, School of Electrical and Electronic Engineering, Huazhong University of Science and Technology, Wuhan 430074, China*
[2] *Forschungszentrum Jülich GmbH, Institut für Energie- und Klimaforschung—Plasmaphysik, Partner of the Trilateral Euregio Cluster (TEC), Jülich 52425, Germany*
[3] *Institute of Plasma Physics, Chinese Academy of Sciences, Hefei 230031, China*
[4] *Southwestern Institute of Physics, Chengdu 610041, China*
[5] *Department of Applied Physics, College of Science, Donghua University, Shanghai 201620, China*
[6] *Graduate School of Advanced Science and Engineering, Hiroshima University, 739-8527, Higashi-Hiroshima, Japan*

[*] Email: y.liang@fz-juelich.de

keywords: Divertor, tokamak, magnetically confined fusion

Abstract

Developing advanced magnetic divertor configurations to address the coupling of heat and particle exhaust with impurity control is one of the major challenges currently constraining the further development of fusion research, and therefore has become the focus of extensive attention in recent years. In J-TEXT, several new divertor configurations, including the high-field-side single-null poloidal divertor and the island divertor, as well as their associated fundamental edge divertor plasma physics have recently been investigated. The purpose of this paper is to briefly summarize the latest progress and achievements in this relevant research field on J-TEXT in the past few years.

1. Introduction

1.1. State of the art of fusion energy research

Since the beginning of the 21st century, fusion research has entered a research era focusing on long-pulse steady-state high-performance integrated scenario development. Several large superconducting fusion devices, such as LHD [1] in Japan, EAST [2] in China, KSTAR [3] in Korea, W7-X [4] in Germany, and WEST [5] in France, have been put into operation one after another. However, the results

from these experiments suggest that overheating of the target plate and impurity accumulation in the plasma core tend to occur once the operating domain is extended to the high power long-pulse steady-state H-mode plasma regime, especially when using an ITER-like tungsten divertor and metallic plasma-facing components (PFCs) [6]. To date, we recognize more clearly than ever that the coupling of heat and particle exhaust with impurity control is one of the most difficult bottlenecks restricting further development of fusion research, and this problem therefore has become the focus of extensive attention in recent years.

1.2. Divertor physics and challenges

The standard poloidal divertor, characterized by a single magnetic field null (X-point) located in the divertor region and two poloidal legs intersecting with the divertor at the strike points, has been developed on many devices to handle power and particle/impurity exhaust and has enabled significant progress in tokamak physics studies [7]. Four critical divertor physics issues, which include *i) power exhaust; ii) D/T and He pumping; iii) reduction of impurity production (source); and iv) impurity screening by the divertor scrape-off layer (SOL)*, have been identified and well investigated. Although the standard poloidal divertor configuration has been planned for ITER, it has been recognized that this concept might be problematic for the high-performance era of ITER operation, and could be inappropriate for a future reactor.

For a conduction-dominated SOL, the basic scaling of the power decay length, λ_q, is given by

$$\lambda_q \approx \pi q R \sqrt{\frac{\chi_\perp}{\chi_\parallel}}; \tag{1}$$

Here, q is the edge safety factor, which is inversely proportional to the plasma toroidal current, I_p, or the strength of the poloidal magnetic field, B_ϑ. R is the major radius of the plasma. $\chi_\parallel$ and $\chi_\perp$ are the thermal diffusion coefficients in the direction parallel and perpendicular to the field lines, respectively. The first three items in the right side of the equation (1) represent approximately the field-line connection length, $L_\parallel$, in the SOL, which is determined by the magnetic configuration and the structure of the divertor target plate.

Due to the significant anisotropic transport effects inside magnetized hot plasmas, where the plasma transport along the field lines is several orders of magnitude higher than the cross-field transport, the plasma parameter profiles decay rapidly inside the SOL, which causes a thin power decay length. For ITER and future fusion reactors, there will be a heat flow of the order of 100 megawatts from the plasma core into the SOL, and most of the heat will be exhausted through the divertor. The λ_q for ITER predicted based on empirical scalings is only about 1 mm, resulting in serious peak value of about 50 MW/m^2 for the steady-state heat load, far exceeding the limit of existing materials (~10 MW/m^2) [8]. Therefore, to sustain the steady-state high performance burning plasma operation in a future fusion reactor, it is of great significance to both increase the power deposition area of the divertor plate and reduce the thermal load power flowing to the target plate at the same time. In order to meet this challenge, the following key aspects related to fundamental physics research on advanced divertor configuration have to be carried out:

- ***Magnetic topology**:* By optimizing the magnetic configuration and the structure of the target plate, the magnetic field lines in the SOL are expanded or lengthened, thereby increasing the deposition area of the thermal load on the target plate;
- ***Plasma transport**:* Increase the effective radial transport of heat and particles and reduce the peak heat load of the target plate; Explore the divertor and the SOL plasma transport physics and optimize further the impurity screening effect.
- ***Heat load dissipation**:* By seeding impurities at the plasma boundary or increasing the plasma density, the total exhaust power, including alpha particle heating and external heating power, should be dissipated as much as possible before being transmitted from the core to the wall, so that the temperature of the first wall can be controlled at a safe level.

In principle, those three issues are interconnected with each other. For a standard poloidal X-point divertor plasma, assuming that the total conductive power flowing into the SOL is balanced by volumetric losses, a simple zero-order detachment criterion [7] can be defined as:

$$\frac{14}{3} C_Z L_Z n_u^2 L_\parallel \approx q_u; \tag{2}$$

where C_Z is the impurity fraction, L_Z is the plasma radiation efficiency, and q_u is the parallel upstream heat flux. Therefore, increasing the field-line connection length at the SOL will facilitate the expansion of the divertor wetted area, as well as easy access of detachment with lower upstream plasma density, n_u.

1.3. Existing advances divertor configurations and open questions

In addition, there are still two essential technical challenges that have to be solved:

- Core-edge integration, which develops and demonstrates dissipative/detached divertor solutions for power and particle control sufficient for extrapolation to power plant conditions;
- Power exhaust solutions taking into account both steady-state and transient heat loads.

These tasks have been recognized as much more complicated problems due to the non-linear coupling of multiple physical processes over a wide range of overlapping spatial and temporal scales for long-pulse high performance plasma scenario development. Explorations of new divertor configurations as well as long-pulse demonstrations of sustained high performance plasma operation with integration of the optimized core-edge coupling and power exhaust solutions have been carried out in many stellarator and tokamak devices [6, 9-13].

In stellarators, both the helical divertor on LHD [14] and the island divertors [15] on W7-AS and W7-X, featuring a three-dimensional (3D) edge magnetic configuration and longer field-line connection lengths at the SOL (in the magnitude of 10^2 - 10^3 m, much longer than the electron mean free path), have demonstrated excellent performances in obtaining either stable strongly radiating divertor plasmas or steady-state full detachment. During the first W7-X high-performance experimental campaign OP1.2, full divertor power detachment has been established and sustained stably. Furthermore, a new record of the

triple product of 6.4×10^{19} keV s m^{-3} for stellarator plasmas has been achieved with pellet injections in a standard island divertor configuration on W7-X. Those results demonstrated good core-edge integration properties of the island divertor concept for stellarator plasma operation.

Recently, a new resilient divertor concept, the so-called non-resonant divertor [16], has been designed for advanced stellarators optimized for reduced neo-classical transport. A feature of this divertor concept is that the locations of the strike points on divertor targets are not strongly affected as the plasma configuration varies (for example due to the inclusion of plasma current).

In tokamaks, two major categories of two-dimensional (2D) advanced poloidal divertor configurations have been developed, including

- high-order null divertors, such as the snowflake and the cloverleaf divertors;
- High-flux expansion and long poloidal leg divertors with multiple X-points, such as the Super-X divertor and the X-point target divertor.

The geometric features of the 2D advanced poloidal divertor configurations and their profound impacts to improve certain detachment characteristics have been recently validated by experiments and modelling on TCV [17], DIII-D [18], and EAST [19]. The experimental observations show more complicated edge transport mechanisms eclipsing the edge impurity transport analysis using the 2D fluid models, and raise many open questions on the fundamental physics of divertor plasmas, such as neoclassical drift effects and their impact on the upstream profiles, inner-outer /up-down divertor balance and divertor power decay length and detachment. On the long-legged and Super-X divertor configurations [20], the upcoming MAST Upgrade experiment will provide critical data not only on the physics but also on engineering performance. However, none of these 2D advanced poloidal divertor concepts can decouple the significant inverse relationship between the plasma toroidal current and the divertor power decay length.

The dynamic ergodic divertor (DED) concept [11, 12], characterized with formation of a proper 3D edge ergodic zone, an area of open magnetic field lines, a laminar zone, and a tangle structure at plasma boundary, has been introduced in the TEXTOR tokamak plasma by applying helical magnetic field perturbations resonating at the q=3 rational magnetic flux surface. The toroidal symmetry of the edge plasma profiles, as well as the heat and particle flux distributions on the divertor target plate was found to be broken. A prominent feature of the ergodic divertor is the ability to control the edge plasma transport, as well as to mitigate/suppress transient heat loads caused by the edge plasma instability, such as edge localized modes (ELMs) in H-mode plasmas [20-24].

It is foreseen that more and more upcoming new experiments and devices will contribute to the development of advanced magnetic divertor configuration, such as HL-2M [25], and DTT [26]. These experiments should enable development of an integrated divertor solution that may be based on one of the reviewed magnetic configurations, advanced target technologies, and compatibility with the core plasma requirements.

1.4. The J-TEXT tokamak

The Joint-Texas Experimental tokamak (J-TEXT) [28], formerly known as TEXT/TEXT-U [29], was moved from the University of Texas at Austin to Huazhong University of Science and Technology in 2004. It is a conventional middle-sized tokamak with a major radius R_0 = 1.05 m, minor radius a = 25–29 cm and the toroidal magnetic field, B_t, up to 3.0 T. Since it resumed operation in 2007, a set of new saddle coils including 24 (3×8) in-vessel and 6 external coils has been installed for flexible adjustment of resonant magnetic perturbations (RMPs) [30]. Furthermore, a 105 GHz electron cyclotron resonant heating system (ECRH) with a maximal power up to 500 kW has been applied for electron-dominated heating [31].

To date, J-TEXT is capable to operate in a variety of plasma configurations including limiter, single- (top, middle or bottom) or double-null high-field-side (HFS) divertor, and island divertor [32]. As part of a long-term fusion research roadmap in China, the J-TEXT experimental program aims to develop fundamental physics and control mechanisms of high temperature tokamak plasma confinement and stability in support of successful operation of ITER and the design of future fusion reactors, such as CFETR [33].

1.5. This paper

In past 5 years, a great effort from the J-TEXT team has been oriented towards advanced divertor configurations, and their related fundamental edge divertor plasma physics. The following subtopics have been pursued and will be continued.

- Realize and characterize the high-field-side poloidal divertor plasmas on J-TEXT with a reliable plasma shape and stability control mechanism, and study fundamental physics of the density limit, impurity transport, radiating divertor, detachment, and the impact of E_r on the up-down asymmetry of divertor loads;
- Develop and optimize the island divertor configuration for a tokamak plasma, considering the stability of the edge islands, impurity screening effects, and 3D divertor heat loads;
- Investigate new divertor concepts, such as the formation of a stochastization boundary with either 3D non-axisymmetric SOL current filaments induced by electrode biasing, or with 3D RMP coils in a limiter or HFS poloidal divertor configuration;
- Develop and evaluate modern edge plasma diagnostics measuring the edge turbulence and turbulent transport, upstream and downstream plasma profiles, and 2D distributions of divertor impurities, plasma flow, and radiation.
- Establish and validate an integrated simulation package to calculate plasma MHD equilibrium, edge particle/impurity transport and stability, and divertor heat flux distributions, in order to support high-field-side divertor experiments, which can also properly support island divertor investigations, in which the edge dynamics are dominated by 3D fields.

In this overview paper, the advanced progress and results towards advanced divertor configurations achieved on the J-TEXT tokamak over the last 5 years, especially on the above subtopics, will be presented.

2. Developments of edge, SOL & divertor plasma diagnostics

Various edge diagnostics have been developed to study the edge plasma parameters in the past decade, which support the achievement of advanced divertor configuration studies on J-TEXT through gaining various figures about the edge plasma behavior [34-43]. In this section, a review of these diagnostics, including reciprocating probes, limiter probes, visible imaging systems, and visible spectroscopic diagnostics, is given. An overview of the presented diagnostics is shown in Fig.1. These diagnostics are dedicated to measuring the edge turbulence and turbulent transport, upstream and downstream plasma parameters, and edge plasma flows and impurity distributions. The diagnostics with their respective measurement roles are listed in Table 1.

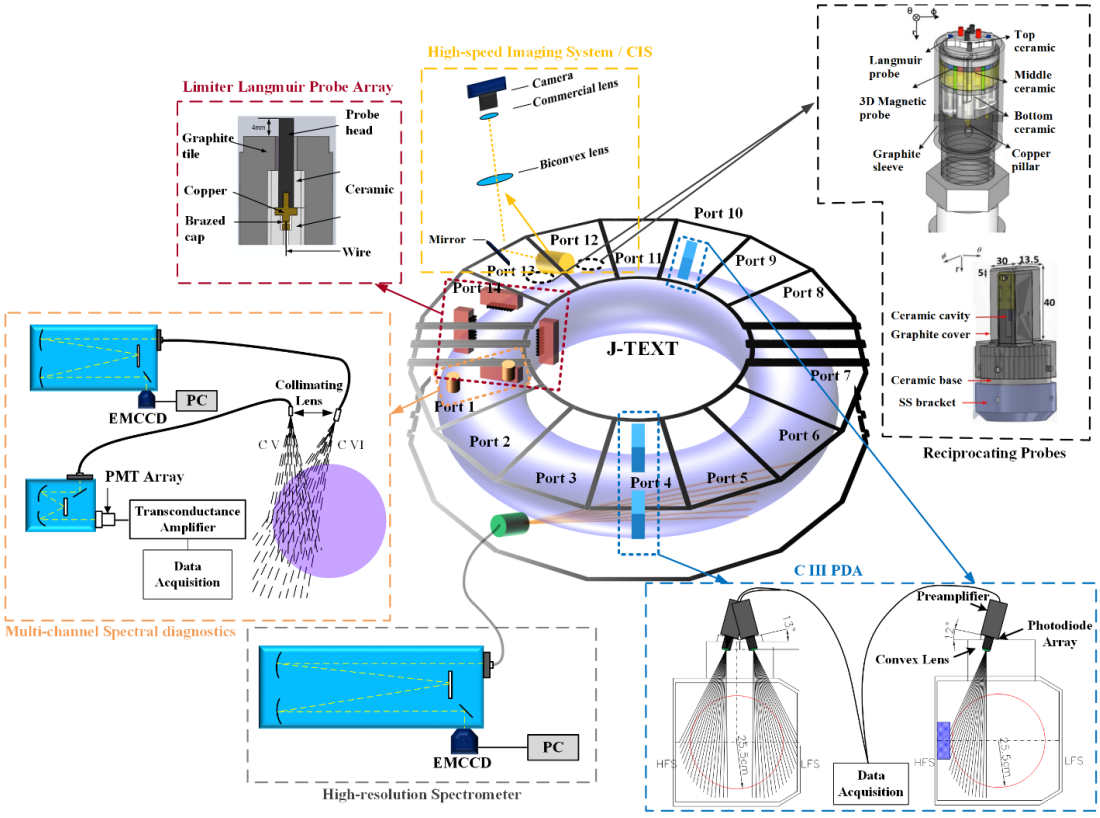

Figure 1 - Layout of edge plasma diagnostics on J-TEXT

Table 1 - Roles of developed edge plasma diagnostics

Diagnostic		**Function**
Reciprocating Probes	*Langmuir Probe*	Upstream n_e, T_e, V_f, and their fluctuations
	Magnetic Probe	Upstream B fluctuations
	Retarding Field Analyzer	T_i
Limiter probes		Downstream n_e, T_e, V_f, and their fluctuations
High-speed imaging system		Visible image
Spectral diagnostics	*C III Photodiode Array*	C III distribution
	High-resolution spectrometer	C III and C V flows
	Multi-channel spectral diagnostic	$n_{C\ V}$ and $n_{C\ VI}$ distribution
	Doppler coherence imaging spectroscopy	$I_{C\ III}$ image, $V_{C\ III}$ image

2.1 Reciprocating Probes

Two sets of reciprocating manipulators are installed at the top windows of two different toroidal positions, port #12 and port #13. These manipulators have a maximum plunge length of 5 cm with a typical speed of about 1 m/s. Several types of probe heads are developed compatible with the manipulators to measure the local plasma parameters at the edge region.

2.1.1 Langmuir-magnetic Probe

The Langmuir probe is commonly applied in tokamak devices [34]. Its configuration was also initially developed on J-TEXT, providing data on electron density and temperature, the floating potential, and fluctuations of these quantities in the boundary region with a temporal resolution of 0.5 μs.

A magnetic probe array was developed to measure the local magnetic fluctuations at the plasma edge [35]. This magnetic probe array consists of four 2D magnetic probes, detecting local poloidal and radial magnetic fields at the plasma edge within the last closed flux surface (LCFS).

Finally, this probe was updated with a composition of Langmuir and magnetic probes, named “Combined Langmuir-Magnetic Probe” (CLMP) [36]. As shown in Fig.1, the Langmuir probe is on the top ceramic, with eight graphite probe pins distributed in two stages. Stage #2 is 3 mm higher than stage #1, so that the probe pins on different stages can obtain electrostatic signals at different radial positions. The middle ceramic holds the 3D magnetic probe, which is made of enamelled copper wire with an outer diameter of 0.23 mm wound on the middle ceramic skeleton. Specific cuts are embedded into the graphite sleeve to minimize the impact of eddy currents.

2.1.2 Retarding Field Analyzer (RFA)

The ion energy transport in the SOL is of importance in understanding plasma-surface interaction [37]. To directly measure the ion temperature, a bidirectional

RFA is employed on J-TEXT. The schematic of the RFA is shown in Fig.2 (a). The RFA array (the slit plate, two grids, and collector) is aligned along the magnetic field. A negatively biased slit plate repels most of the thermal plasma electrons and allows for the ions to enter the analyzer. The transmitted ions encounter Grid 1 and are selectively retarded by the sweep voltage, $V_{Grid\ 1}$. Grid 2 is biased negatively enough to suppress secondary electrons emitted from the collector and the slit plate due to ion impacts.

The basic RFA and the eiRFA (for electron and ion temperature measurement) schemes were implemented in succession [38]. For the RFA scheme, as presented in Fig.2 (b), the ion temperature could be evaluated by sweeping the collector voltage and current matching Maxwellian distribution. For the eiRFA application, as shown in Fig.2 (c), the slit plate is biased with an AC voltage, which is used for scanning the SP-I-V (single probe acted by the slit plate), as well as for sifting the ions into the eiRFA. For this scheme, grid 1 is biased negatively to repel the electrons. Bias arrangements and functions of Grid 2 and collector remain unchanged.

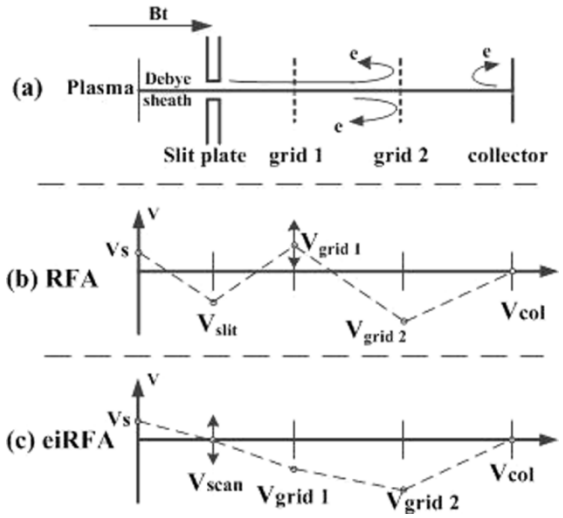

Figure 2 - (a) The schematic of the basic principle of RFA operation. Bias arrangements for (b) the traditional RFA in ion analysis mode and (c) the eiRFA analysis mode.[38]

The linear relations between V_{scan} and ln (I) can be found and the T_e and T_i can be obtained from the slopes of ln ($I_{scan,e}$) − V_{scan} and ln ($_{Iscan,i}$) − V_{scan}, respectively.

2.2 Limiter probes

The limiter target electrostatic measurement system, including limiter grounding current sensors and Langmuir probes, was newly developed for the measurement of the limiter target area [39]. Additionally, a limiter Langmuir probe array (LLPA) embedded in graphite tiles of limiters was also built for a more localized measurement. The LLPA consists of fifty-four graphite probes, which are arranged symmetrically with respect to the mid-plane. The probes are distributed in 8mm spaced pairs, with the distance between two adjacent pairs being 25 mm. This dense distribution at the HFS is beneficial to investigating the electrostatic parameters of the HFS divertor X-point. Besides the different poloidal positions, the radial position of the probe tip relative to the LCFS are also different. A coaxial line transmits the signal to the data acquisition system in

a nearby isolated cabinet through the sampling circuit. The sampling rate of a single acquisition channel is up to 750 kHz.

2.3 Non-invasive diagnostics

2.3.1 Visible light high-speed imaging system

A visible light high-speed imaging system (VLHIS) was installed on the J-TEXT tokamak to measure the spatial distribution of visible light in the vacuum chamber [40]. This system views the plasma tangentially from an outer port at the height of the vacuum vessel's mid-plane. In order to capture the plasma images of the whole poloidal cross-section of the vacuum vessel, the camera system is mounted at a tangential window on the mid-plane of the vacuum vessel, looking clockwise. A customized optical system was designed to move the CCD camera away from the window, avoiding disturbances on the camera caused by the strong toroidal magnetic field. This optical system includes four components, two biconvex lenses, a commercial lens, and a reflector. One biconvex lens1 (f=80 mm) is placed close to the tangential window to increase the field of view because the tangential window could occlude some light from the low field side (LFS) or the HFS.

2.3.2 High-resolution ultraviolet/visible spectrometer

A high-resolution ultraviolet/visible spectroscopic system was developed to measure the rotation velocity of light impurities in the edge region of J-TEXT [41,42]. Carbon V (C-V 227.09 nm) and carbon III (C-III 229.69 nm) were chosen as the lines to be measured. These two lines can be acquired by the spectrometer together. Therefore the two ions' velocities can be obtained simultaneously.

The spectroscopy system (shown in Fig. 1) consists of a 1.33 m focal length monochromator with an 1800 g/mm grating, an EMCCD camera with 1024 × 1024 pixels, and a fiber optic light collection system with 17 viewing channels. Sixteen of these viewing channels, each channel consisting of two fibers (diameter = 200 μm), are used for toroidal rotation measurement based on the Doppler shift. The mean diameter of the viewing cones inside the plasma is about 8 mm, which provides the good spatial resolution necessary for rotation velocity measurements. A channel is dedicated to the reference channel giving zero velocity, for which the line of sight is perpendicular to the horizontal plane and passes through the plasma centre.

A spatial deconvolution technique is used to obtain the local rotation velocity, since the collected light from plasma is line-integrated. In this technique, the plasma cross-section is divided into several layers according to the number of viewing channels, and the parameters, including emission intensity, rotation velocity, and ion temperature, are assumed to be symmetric in the toroidal direction. The plasma parameters of the inner layers are determined by removing the contribution from the outer layers. Hence, the relative differences among measurement channels in spectral responsibility, wavelength deviation, and instrument function must be known through careful calibration. Here, the bulk plasma is applied as the calibration light source for determining the spectral responsiveness and wavelength deviation.

2.3.3 Spectroscopic diagnostics for edge impurity studies

Several visible/UV spectroscopic diagnostics are composed to form a light impurity diagnostic system, providing several impurity (for carbon ions, specifically) radiation profile measurements in the plasma edge region [43]. It consists of two carbon III (C-III 464.7 nm) photodiode arrays (PDAs), one carbon V (C-V 227.09 nm) diagnostic, and one carbon VI (C-VI 529.26 nm) diagnostic.

The two PDAs are identical. Each is configured with an 18-channel photodiode array, a specified front C-III filter (centre wavelength of 466 nm, bandwidth of 5 nm), a collimator, and an in-built amplifier. Two PDAs are installed at port 4, dedicated to measuring the C-III emission in the HFS and LFS. The spatial resolution, time resolution, and coverage area of the C-III diagnostic are 13 mm, 100 μs, and r_{chord} = 7−29 cm, respectively.

The C-V diagnostic was developed to measure the emission profile of C-V in the HFS region, shown in the orange area in Fig.1. This system consists of a 12-core fiber bundle with a core diameter of 400 μm for light collection, an aberration-corrected monochromator, one photomultiplier tube (PMT) array, and an amplifier. The monochromator with a focal length of 300mm, a grating of 1200 g/mm, and an effective aperture of f/4.2, can be used to select specific wavelengths (usually for carbon V 227.09nm). The PMT is used to convert light into current signals, which are then converted to voltage signals via the amplifier. The temporal resolution, spatial resolution, and coverage area of the array are 0.1 ms, 12 mm, and r_{chord} = 25.5 cm to 12 cm, respectively.

The configuration of the C-VI diagnostic is similar to the high-resolution ultraviolet/visible spectrometer. It consists of a 10-core fiber bundle with a core diameter of 200 μm for light collection, an aberration-corrected monochromator with a focal length of 750 mm for light dispersion, and an EMCCD camera with 512 × 512 pixels for light detection. The grating is spaced at 1200 g/mm. The wavelength range is 190-2100 nm, but the central wavelength is set to 529.3nm to measure the C-VI line in common operation. Since the distribution of C-VI radiation is relatively wide, a acceptance angle of 30 degrees is applied to achieve an appropriate viewing coverage area to observe C-VI behavior in the HFS region. The temporal resolution is mainly determined by the radiation intensity and is usually set to 10 ms.

2.3.4 Doppler coherence imaging spectroscopy

A doppler coherence imaging spectroscopy (CIS) has been installed on J-TEXT tokamak to provide the 2D profile of the emissivity and the flow of C-III impurity ions via the Doppler shift of their characteristic spectrum. It shares the same window with VLHIS (which is presented in section 2.3.1). The imaging process relies on commercial lenses, achieving the system's focal length of 70 mm. A custom band-pass filter is used to isolate the target spectral line (C-III 464.7 nm). The key part of the CIS diagnostic is a static polarization interferometer, which is based on spatial multiplexing techniques with a spatially varied phase delay (along one detector dimension). Adding the Phantom V2012 high-speed camera, the system can reach a temporal resolution of 5ms, a spatial resolution up to ~ 0.8 mm in the horizontal direction, and ~ 9 mm in the vertical direction. The emissivity and the flow profiles are evaluated through a specifically developed

spatial inversion, based on Tikhonov method, which was successfully developed and applied to reconstruct the topography of flow on J-TEXT.

2.3.5 Discussion & future challenges

By combining these diagnostics, many physics processes linking to the formation of divertor plasmas, could be deduced. The edge plasma temperature, and electron and the edge impurity intensity are used to understand the plasma and wall interactions. The edge electrical field and edge flow could be applied to identify the formation of the X point. Adding the turbulence information, which is represented by the fluctuations of plasma parameters, the transition of edge plasma transport is involved.

To depict a clearer image assisting the deeper study of the various plasma behaviors in the unique divertor configurations on J-TEXT, the edge diagnostics are kept in continuous improvement with more measurement channels in development, such as the C III PDAs and target probes. To interpret the large data collections provided by these systems, a comprehensive data flow that combines various diagnostics needs to be developed.

3. Integration of numerical simulations for edge & divertor plasma transport

To keep up with the shifting demand from fundamental research into operational scenario development, simulation development in fusion is trending towards integrated modelling approaches, where individual physics codes focusing on a single aspect of plasma physics (MHD equilibrium, instabilities, plasma transport, impurity transport, plasma-wall-interaction, wall evolution) are increasingly employed together to reproduce experimental scenarios and allow the planning of future devices and their operation. This shift has substantially increased the validation burden on the individual physics codes, as validating a single aspect of a multi-stage model can only be done once sufficient trust is established in its other stages.

In the recent years, substantial progress was made challenging and improving the accuracy of workhorse codes for integrated scenario applications. In the plasma edge, this primarily requires tying together the individual aspects of edge magnetic field evolution (Bootstrap current, MHD equilibrium, MHD instability), main plasma transport, impurity transport & radiation, and plasma-wall interaction, into models for advanced divertor configurations.

The advancements discussed in this section can be roughly categorized into four different areas:

- 3D edge field modeling: In advanced divertor scenarios, accurate prediction of transport and wall interaction requires precise knowledge of the edge magnetic field structure. Here, the application of full 3D equilibrium and instability codes has substantially increased the precision of predicted and reconstructed magnetic topologies.
- 3D transport modeling: RMP-perturbed poloidal divertors and island divertors require transport codes capable of full 3D simulation. In this

area, substantial advances were made by integrating codes before mainly developed for Stellarator application with Tokamak scenarios.

- Accurate transport and PWI modeling for advanced divertor configurations: Novel divertor configurations such as symmetric high-field side divertors, snowflake configurations, or the Super-X are particularly sensitive to drift effects, which are particularly challenging to model correctly. Here, significant progress has been made to employ J-TEXT's high-field-side divertor (whose inherent up-down symmetry makes it uniquely suitable for drift effect studies) as a benchmarking facility for code validation.
- Active control of unstable magnetic configurations: Tokamak operation regularly requires trading plasma stability against performance. Therefore, advanced control systems incorporating knowledge about the plasma behavior provide extremely attractive options to improve device performance. Advances were made in stabilizing high-field-side and low-q plasmas in a controlled experiment environment through modeling-driven control schemes.

3.13D Magnetic equilibrium modeling

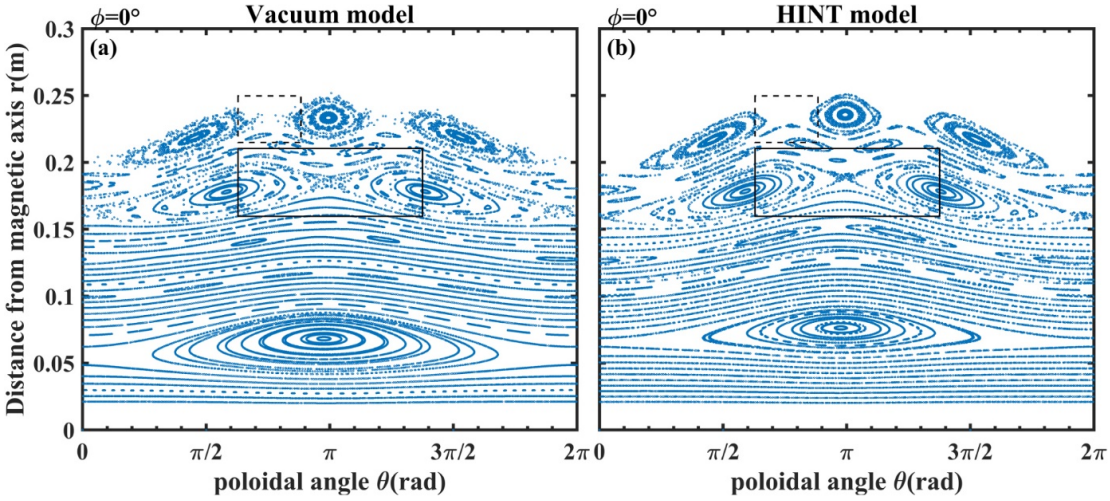

Figure 3 Poincaré plots of the vacuum approximation (2D MHD equilibrium + RMP) and HINT (3D MHD equilibrium) model at Φ = 0° for I_{RMP} = 3 kA. (a) Vacuum model, (b) HINT model. The solid rectangle marks an X-point of the 2/1 magnetic island chain and the dashed rectangle marks an X-point of 3/1 magnetic islands [45].

While 2D magnetic equilibria are well-suited for equilibrium reconstruction in Tokamaks, they cannot capture the behavior of 3D fields interacting with the main plasma. Therefore, these models are insufficient for proper reconstruction of the island divertor's magnetic geometry. Up to this point, J-TEXT's divertor field distributions were obtained by superimposing the RMP coil fields directly on top of the (plasma-driven) equilibrium magnetic fields. This approach is called the "vacuum approximation", as it neglects the interaction between the main plasma and the RMP fields. Such an approach fails to consider screening effects from the main plasma which produce a nonlinear response to the externally applied field.

The predictions from such a vacuum assumption model were now refined upon by the incorporation of the full-field nonlinear resistive MHD model HINT [44, 45]. These calculations revealed local deviations in the current density around and inside the magnetic islands (see Fig. 3), which induced significant changes in island size, position, and shape between full-field MHD and the vacuum assumption. The prediction of these deviations could in turn be backed up by experimental evidence from J-TEXT plasma discharges.

3.2 3D plasma & impurity transport modeling

In order to leverage the full 3D knowledge of the magnetic configuration, the associated transport codes also need to be able to perform full 3D simulation. Due to the traditional focus on poloidal divertor operation, this is an area traditionally somewhat neglected in Tokamak research (with a few exceptions such as TEXTOR-DED), while being of extremely high relevance for Stellarators.

For J-TEXT, the recent research in this area was focused on integrating the EMC3-EIRENE code package into Tokamak simulation workflows. EMC3-EIRENE is a coupled code combining the 3D edge plasma fluid Monte-Carlo code EMC3 with the impurity Monte Carlo model EIRENE. EMC3-EIRENE can operate in non-axisymmetric plasmas, making it a popular edge transport code for Stellarators. As an initial benchmark application, EMC3-EIRENE was employed to investigate the relationship between the exact magnetic geometry of the divertor (particularly the X-point location) and the impurity distribution and radiation in the plasma edge (see Fig. 4 for an example). Comparisons with high-density experiments showed a reasonable agreement between simulations and modeling, demonstrating the readiness of the code package (particularly concerning its strong requirements on grid generation) for Tokamak divertor topologies [46].

Another important aspect of edge transport modeling is the assessment of heat loads onto the plasma-facing components. Whereas axisymmetric configurations

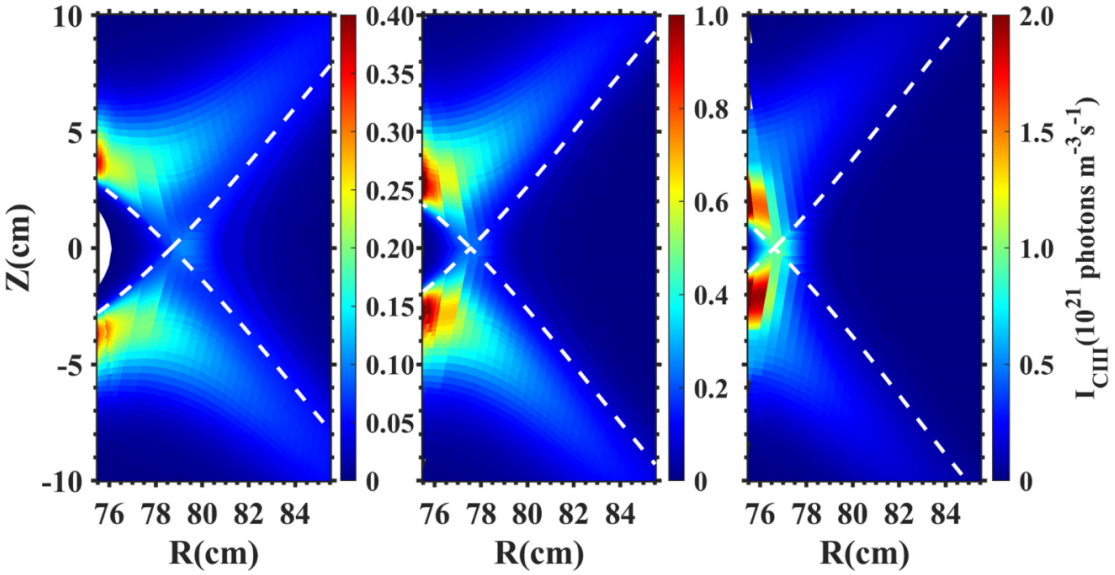

Figure 4 C-III radiation intensity distributions simulated with EMC3-EIRENE at distinct divertor coil currents of 15, 12, and 10kA. The dashed lines represent the locations of the separatrix [46].

usually only produce a set of similarly symmetric strike-lines, the introduction of 3D fields into the magnetic geometry substantially complicates the resulting heat load patterns. While 3D edge transport codes such as EMC3-EIRENE are fully capable of producing heat load distributions on their domain boundaries, these codes are primarily designed to investigate the edge plasma volume. On the one hand side, this imposes strict quality requirements on the grid generation process (which hinder automation and bulk analysis of many magnetic configurations), while, on the other hand side, this also limits the expressiveness of the codes regarding the exact PFC geometry (by restricting boundary meshes onto grid cell interfaces).

To remedy these issues, a purpose-built Monte-Carlo proxy model was realized based on simple anisotropic diffusion (with parallel/perpendicular diffusion coefficient ratios of about 10^6 to 10^7) [47]. The linearity of this model implies that all test packets could be traced independently, eliminating the need for any sort of accumulation grid. By directly relying on high-resolution meshes for the boundary representation, this model could produce fine-grained predictions of heat loads distributions. Recent investigations on the Wendelstein 7-X (W7-X) stellarator revealed the necessity of a diffusive parallel transport mechanism, as counter-streaming flows (which are rare in axisymmetric geometries) can have significant influence on the heat load distribution. After successful application on W7-X, this anisotropic diffusion model is currently in application on J-TEXT for investigation of the island divertor configuration.

3.3 Accurate transport and PWI modeling for advanced divertor configurations

In addition to the investigation of 3D fields, efforts were also made to improve the understanding and accurate plasma state reconstruction of advanced axisymmetric divertor scenarios. Modern divertor configurations such as Snowflake, Super-X, High-Field-Side divertors, or double-null configurations, are particularly substantially more sensitive to drift effects when compared to classical single-null poloidal divertors.

A code particularly suited for analyzing drift-sensitive edge transport scenarios is the SOLPS-ITER package. Like EMC3-EIRENE, SOLPS-ITER is a combination of dedicated models for the edge plasma transport and the impurity transport. However, instead of relying on EMC3, SOLPS-ITER instead uses the B2.5 plasma solver. B2.5 is a fast 2D transport solver for axisymmetric configurations, which features a particularly comprehensive physics model, including terms for main plasma drifts.

While the application of SOLPS-ITER to J-TEXT is actively underway (focusing in particular on the high-field side poloidal divertor scenarios), it was also employed to investigate experimental scenarios on the close-by EAST Tokamak [48]. There, it was used to provide a detailed study relating the magnetic field direction with SOL density profiles and fall-off lengths, which made wide usage on the code's comprehensive and detailed physics model.

3.4 Plasma instability modeling

One major obstacle to operation with a high-field-side divertor is the radial instability of the high-field-side middle-single-null configuration. In order to define and extend the operational window surrounding this instability, a filament-based force-balance model was developed to simulate the dynamic radial movement of the plasma in a feedback-controlled environment (where feedback was provided via the vertical field coils). Results from this indication showed that the HFS divertor configuration could be sufficiently stabilized for active feedback control by shifting the magnetic axis location slightly outward compared to standard operation [49].

The instability model was then expanded upon by incorporating the dynamic behavior of the feedback control system itself into the simulation. Through joint simulation of both the instability and the feedback control, the stability domain of the control scheme could be determined both in configuration space (axis position, plasma beta) and the feedback control parameters. This analysis revealed optimal response parameters for the feedback control system, which allowed for more effective suppression of the radial instability and an extended operation space for the HFS divertor configuration [50].

The second focus of instability research was the investigation of low-q plasma stabilization through external 3D fields. In the recent years, investigating the impact of 3D magnetic perturbations on plasma stability has become a major focus of J-TEXT research. A major instability is the ideal kink mode, which usually imposes a lower boundary of $q_{edge} >= 2$ on Tokamak operation. For J-TEXT, the behavior of these plasmas was investigated with the MIPS code. MIPS incorporates a non-linear resistive 3D MHD model, which includes the effects of magnetic reconnection and nonlinearities due to pressure profile redistribution.

By analyzing the behavior of the kink mode in an external 3D field, it was found that a pair of opposite iota=1 coils can be used to stabilize the kink mode and suppress its growth by adding a small background m=2, n=2 component to the edge magnetic field [51]. Such a coil pair might be used in the near future on J-TEXT to experimentally investigate the stabilization of the low-q regime.

3.5 Discussion & future challenges

The divertor configurations of J-TEXT present highly attractive targets to benchmark integrated edge modeling, particularly due to its combination of agile small-scale operation and a wide array of advanced magnetic configurations available. On this test bed, the individual components required for comprehensive edge modeling have shown promising benchmarking results and good capability to handle unusual magnetic configurations.

The next step will now be to integrate all these 3D modeling workflows into a single, unified, analysis approach. This will require an efficient exchange of data between the individual codes and tight coordination between individual researchers, and care will have to be taken in how to achieve a consistent picture in the different models. However, thanks to the performed in-depth validation studies, this integration effort can now take place with a strong confidence in the individual codes themselves.

4. High-field-side poloidal divertor configuration

At the end of 2018, a special poloidal divertor configuration with a midplane single null at the high-field side (HFS-MSN) has been successfully realized for the first time on J-TEXT by utilizing three sets of divertor coils (DV) and two sets of bias coils (BS). These DV and BS coils located in the inner cylinder were carried over from the past TEXT-U tokamak. By tuning the amplitude and orientation of the current flowing in each of these coils, it is possible to flexibly change the divertor configuration from single-null (SN) to double-null (DN) and the X-point location as well during the discharge. To maximize the heat load handling capability for the divertor plasma operation, a SiC-coated graphite divertor target fully covering the entire inner wall has been newly constructed. To date, J-TEXT is the only device in the world capable of operating in various different HFS divertor configurations, especially with the HFS-MSN, where the X-point is located in the favourable-curvature area.

Compared with the limiter configuration, the HFS-MSN divertor configuration (an example as shown in Fig. 5) greatly increases the wetted area, and reduces the peak heat flux on the target plate, which may mitigate the sputtering of impurities. In this section, recent approaches in various experiments, including density limit, radiating divertor and detachment on J-TEXT with the HFS-MSN divertor configuration will be highlighted. Furthermore, experiments investigating the impact of E_r on the up-down asymmetry of divertor loads (using the electrode biasing system) will be presented as well.

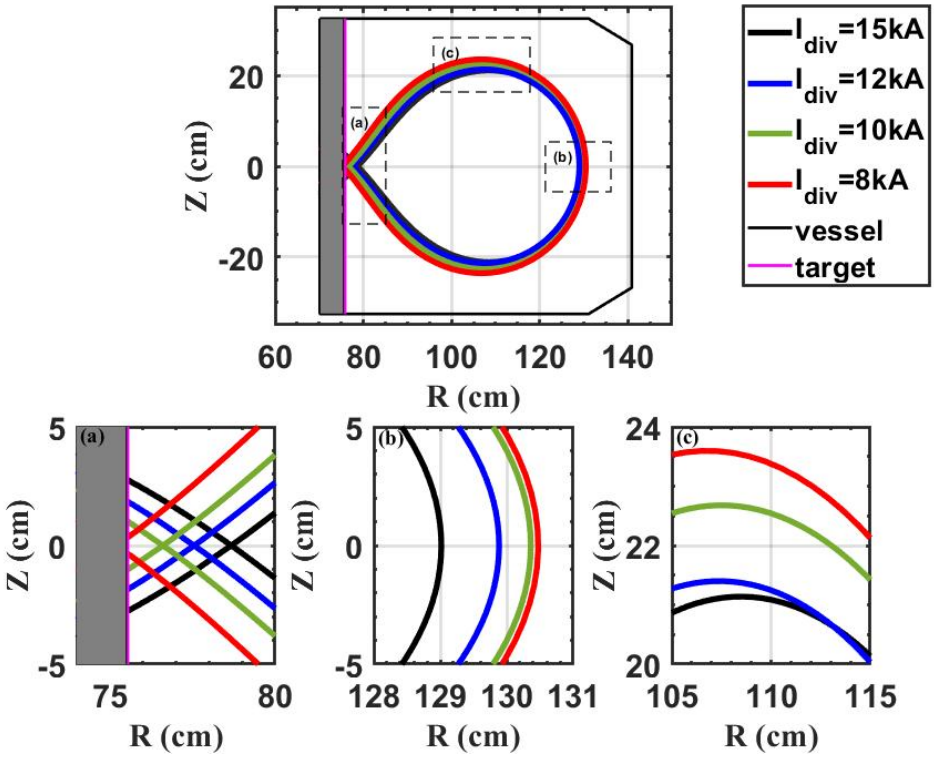

Figure 5. LCFS generated from EFIT for the HFS-MSN divertor configurations with different divertor coil currents and enlarged views of three regions [46]

4.1 Density limit/X-location dependence

Recently, a series of high-density experiments in divertor configuration was carried out on J-TEXT [46]. A significant extension of the density limit from a Greenwald fraction of 0.5 to 0.79 has been achieved by changing the ohmic plasma from the limiter configuration to the HFS-MSN configuration (as shown in Fig. 6). In this experiment, the plasma density was ramped up through gas puffing from the bottom flange. With increasing plasma density, the SOL electron temperature dropped, and the downstream ion saturation flux increased faster than the upstream ion saturation flux, which may result from the radial transport changes with the density ramp-up. Meanwhile the impurity radiation was enhanced, which is helpful in reducing the target heat load. However, under ohmic discharge conditions, the core radiation still dominates even in divertor plasmas, resulting in difficult access to further high-density operation domains.

Moving the X-point away from the divertor target was shown to improve the density limit, and to result in an increase in the peak divertor heat flux and a decrease in the divertor heat flux decay length. Constrained by an open divertor without a neutralizing gas pumping system and low heating power, the high recycling regime has not been observed in the HFS-MSN divertor plasma on J-TEXT. The ratio of the downstream flux to the upstream flux is still linear as the plasma density rises.

In future experiments, the introduction of electron cyclotron resonance heating (ECRH) could help to further increase the edge plasma density and improve the edge plasma and impurity transport. This might enable the device to explore higher plasma density ranges, which would also be of interest to the HFS divertor studies.

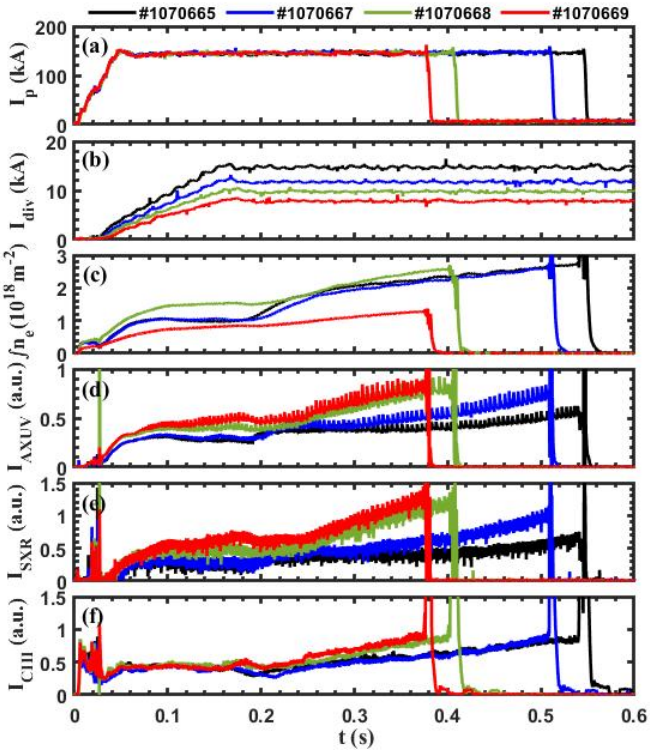

Figure 6. Time evolutions of the operation and plasma parameters with different DV currents.[46]

4.2 Impurity transport/X-location dependence

The SOL impurity screening effect has been observed in the J-TEXT plasma with the HFS-MSN divertor configuration, and it is more favorable when the X-point location is moving away from the target plate. A comparison of the temporal variation of radiation profiles from the density ramp-up discharges with various X-point locations is shown in the Fig. 7. The results show that the radiation intensity in both the core and the SOL is reduced with increasing divertor coil current I_{div} (which means the X-point moves away from the target).

In high-density HFS-MSN divertor plasma experiments, the density-normalized radiation intensity measured by Absolute eXtended UltraVioletl (AXUV) and soft X-ray (SXR) diagnostics was reduced by more than 50% compared to that observed in the limiter configuration.

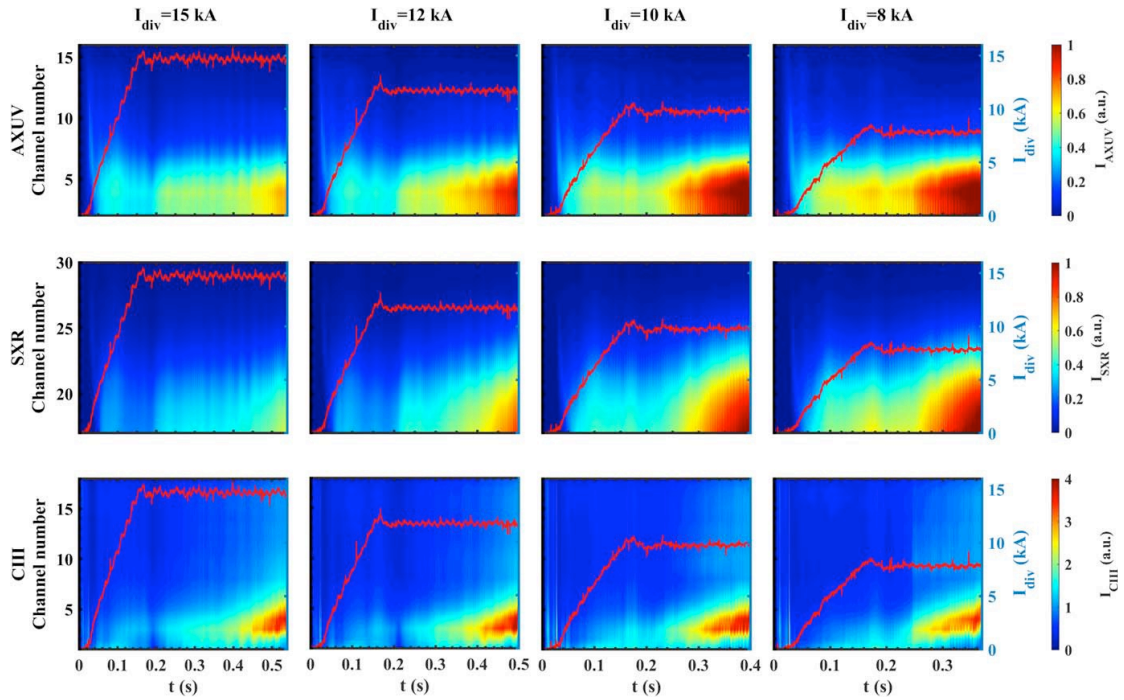

Figure 7. The waveforms of the AXUV, SXR, C−III signals. The red line is the DV current.[46]

The Doppler coherence imaging spectroscopy (CIS) provided two-dimensional radiation signals to investigate the evolution of the C-III radiation distribution near the HFS target before disruption. When comparing the signals at 200ms and before disruption, the C-III radiation distribution is concentrated to the HFS when the density increases, as shown in Fig. 8. Before disruption, the radiation intensity peaks with different I_{div} are near the same location. However, the location relative to the last close flux surface is deeper towards the core due to the X-point being closer towards the target at low I_{div}.

To better understand the underlying physics mechanisms, EMC3-EIRENE was applied to study the SOL plasma transport in HFS mid-plane single-null configurations on J-TEXT. Good qualitative agreements between simulation results and the experimental findings were obtained. The simulation results provided detailed 2D distributions of the main plasma parameters, as shown in Fig. 4.

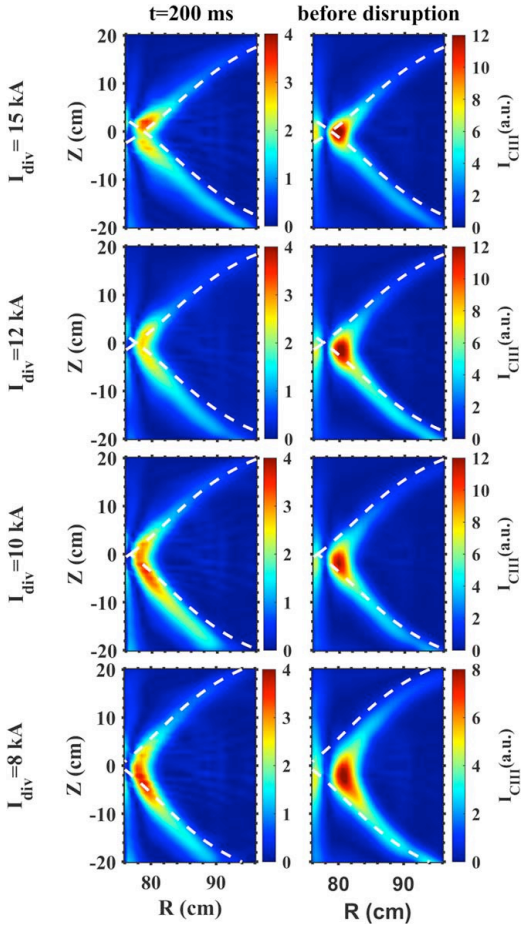

Figure 8. The radiation intensity distribution from CIS. The dashed white line is the separatrix.[46]

4.3 Radiative divertor

Radiative divertors, which dissipate plasma energy by actively controlling impurity radiation at the plasma boundary, have emerged as an attractive technology for reducing the heat load on the divertor plate and reaching detached plasmas in long-pulse high-performance plasma operation. Recent experimental efforts on the majority of existing tokamaks and stellarators have been made to exert finer control over detachment characteristics in order to optimize the reduction of heat flow to the divertor plates while simultaneously minimizing the influence of increased contamination and radiation on energy confinement.

The first experimental investigation of highly radiative divertor and detachment regimes with impurity gas seeding in the HFS-MSN divertor configuration has recently been carried out on J-TEXT. Figure 9 shows an example discharge with methane (CH_4) seeding. In this experiment, the stable HFS-MSN divertor configuration is formed from 0.2s as the divertor current reaches its flat-top. The locations of the upper and lower strike points are around Z_{tar}=±3cm. A gas injection nozzle is embedded on the HFS divertor target plate in the mid-plane, and its location is just in the divertor private flux region. A high-pulse voltage waveform to control the piezoelectric crystal valve was preset at 0.3s for injecting CH_4(red line in Fig. 9(b)). After a delay of about 0.02s (due to the gas tube length), it can be seen that the electron temperature, T_e, drops to around

5eV and the heat flux, q_t, decreases near the strike points at t=0.32s (measured by divertor Langmuir probes). As shown in Fig. 9(f), the temporal evolution of the 2D C-III radiation profiles with CH_4 gas puffing in the divertor region can be observed by a wide-angle visible light high-speed imaging system with a CIII filter [40]. The preliminary results show that the C-III radiation intensity at the lower strike point increases first, then the radiation at the upper strike point increases shortly after, and finally the radiation near the X-point also increases. With a continuous injection of CH_4, the divertor ion saturation current in the far SOL region (around $Z_{tar} = \pm 4.5$cm) continued to increase, as shown in Fig. 9 (d). The plasma line-average density also increased at the same time, and eventually lead to a density limit disruption.

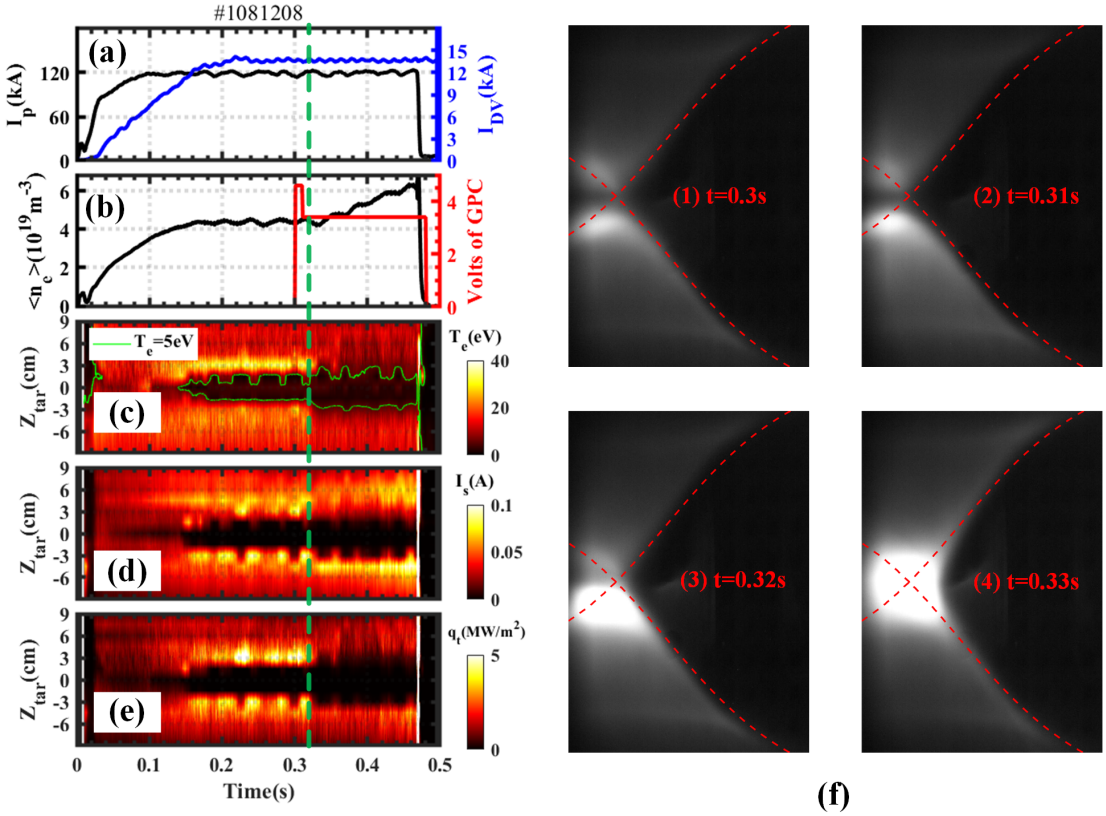

Figure 9. Plasma parameters for a high-density discharge (#1081208) with CH_4 seeding. (a) plasma current I_p (black) and divertor coils current I_{DV} (blue). (b) line-average density $\langle n_e \rangle$ (blue) and control voltage signal of HFS gas-puffing (red). (c) divertor target plate electron temperature, T_e , (d) ion saturation current, I_s , and (e) heat flux, q_t, measured by divertor Langmuir probes. (f) the visible imaging with CIII filter, t=0.3s before CH_4 seeding, and t=0.31s, 0.32s, 0.33s after CH_4 seeding.

4.4 Impact of Er on the up-down asymmetry of divertor loads

The in–out asymmetries of the heat flux and particle flux on the divertor target are key issues for future high-power long-pulse scenario. The asymmetry arises from many factors, mainly including classical drifts (electric and diamagnetic drifts)[52, 53], ballooning instabilities, and Pfirsch–Schlüter (PS) flows [54]. So far, the electric drift $E_r \times B$ has been considered as a primary reason for the in-out asymmetry. Similar to the in-out asymmetry, an obvious up-down asymmetry has been observed in the HFS-MSN divertor configuration on J-TEXT. In this

experiment, the effect of the $E_r \times B$ drift on the up-down asymmetry was investigated by using a movable electrode bias (EB) to modulate the edge E_r.

The discharge parameters are as follows: the toroidal magnetic field $B_t = 2T$, the plasma current $I_p = 120kA$, the divertor coil current $I_{div} = 14kA$, the central line-averaged density $\langle n_e \rangle = 4\times10^{19}m^{-3}$, and the radial position of EB is at $r = 210mm$ (part of EB enters the LCFS). As shown in figure 10(a), the orientation of the biasing voltage can significantly influence the radial field profile. Measurements of the ion saturation current profile (fig. 10(c)) indicates a significant asymmetry in the particle fluxes, which is directly related to the applied bias voltage. A similarly significant response to the biasing application can be seen in the vertical distribution of the H_α radiation intensity measured by a photon detector array (PDA) viewing the HFS (fig. 10 (d)). Without biasing, both I_s and H_α radiation at the upper strike point are stronger than at the lower strike point. Under a positive biasing voltage of +300V, the V_f (fig. 10(b)) of the strike point increases, which indicates that the EB probe has touched the LCFS. The E_r in the SOL points outward and the amplitude increases significantly, so the direction of $E_r \times B$ drift points towards the upper strike point. This results in an increase in the asymmetry of the upper and down strike points. With a negative bias, the phenomenon is opposite to the positive case. In this case, the observed I_s and H_α radiation at the down strike point are higher than the upper strike point, and the asymmetry is reversed.

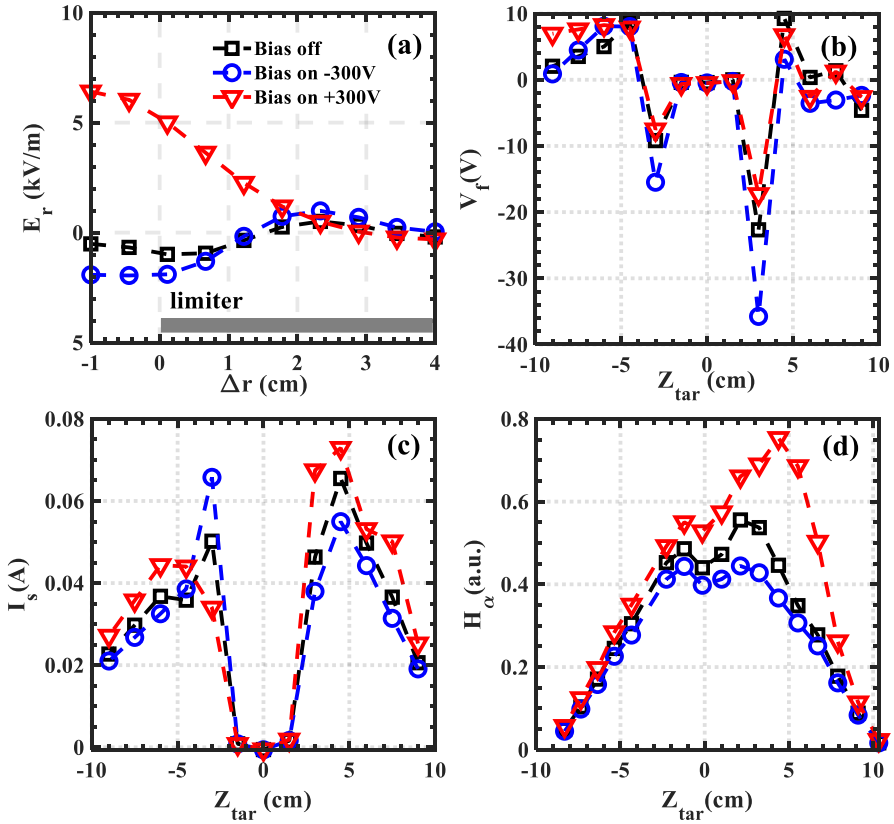

Figure 10. (a) Radial profiles of the radial electric fields E_r measured by reciprocating Langmuir probes, positive value means that the E_r points radially outward; (b) and (c) floating potential V_f and ion saturation current I_s distribution measured by the Langmuir probe array on the HFS divertor plate; (d) vertical distribution of the H_α radiation intensity measured by PDA viewing the HFS.

4.5 Future plans

Concerning the HFS divertor configuration on J-TEXT, the plasma parameter distribution near the divertor target plate and the radiation level near the X-point will be the near-time focus of later experiments. The combination of the X-point and the thermal instability (MARFEs) [12] on the HFS boundary will be further investigated to develop detachment scenarios and associated feedback control technology, aiming to reduce the negative impact of detachment on the plasma confinement and stability of the core. In addition, the existing electrode biasing system will be upgraded, and a biased divertor target will be constructed. After that, experiments with actively control boundary electric field will be carried out to study the effect of E×B drift on the power decay length, detachment and asymmetric heat flow of the upper and lower (inner and outer) target plates. Finally an electrostatic control scheme will be proposed to control the heat load on the divertor target plate.

5. Island divertor configuration

The island divertor, one of multiple attractive advanced divertor concepts, has been successfully applied on the W7-AS stellarator, and further developed on the W7-X stellarator. In the island divertor configuration, the SOL is formed by a group of magnetic islands, which form closed flux tubes around the core plasma. These edge islands are then intersected and cut open by divertor target plates. Compared with the standard poloidal divertor configuration, the island divertor configuration has a weaker correlation with the plasma current and a longer connection length, which results in a wider distribution of heat loads and being also easier to enter stable detachment of divertor operation [55]. Therefore, it is of great interest and significance to apply and explore the island divertor configuration in tokamak plasmas. Recently, a first attempt has been made to form an island divertor configuration in the J-TEXT tokamak. In this section, the characteristics of this J-TEXT island divertor will be presented.

5.1 Formation of island divertor configuration

On J-TEXT, the first island divertor configuration was formed by moving the m/n=3/1 edge island chain outward to intersect with divertor target. Here, m and n are the poloidal and toroidal mode number, respectively. In this experiment, the m/n=3/1 edge magnetic islands were excited by applying RMPs with a dominant m/n = 3/1 component [56,57] in a limiter plasma with an edge safety factor, q_a , slightly over 3. By increasing the plasma current to reduce the edge safety factor, the edge magnetic islands are cut by the divertor target to finally build up the island divertor configuration. An example showing the formation of an island divertor configuration is presented in Fig. 11. When the 3/1 edge islands are gradually opened by the divertor target (t = 0.26 ~ 0.4 s), the main striking-points, indicated by the floating potential measurements (figure 11(g)) from the divertor Langmuir probe arrays, move to two sides (R <

1.05 m and R > 1.05 m) of the divertor target. This reveals that topological differences considerably affect divertor heat-load patterns. Once the 3/1 edge islands are fully moved behind the divertor target, the island divertor configuration is then transformed back to a limiter configuration (t > 0.4 s). The formation of island divertor configuration strongly depends on edge magnetic topologies, or more specifically, the interactions between the edge island and the divertor target. By optimizing the edge magnetic topology and the structure of the target plate, the divertor heat-load distribution could be significantly modified, so as to increase the power deposition area and reduce the peak heat-load. Such optimization processes are being carried out on J-TEXT, leveraging both 3D edge transport modeling and dedicated experiments.

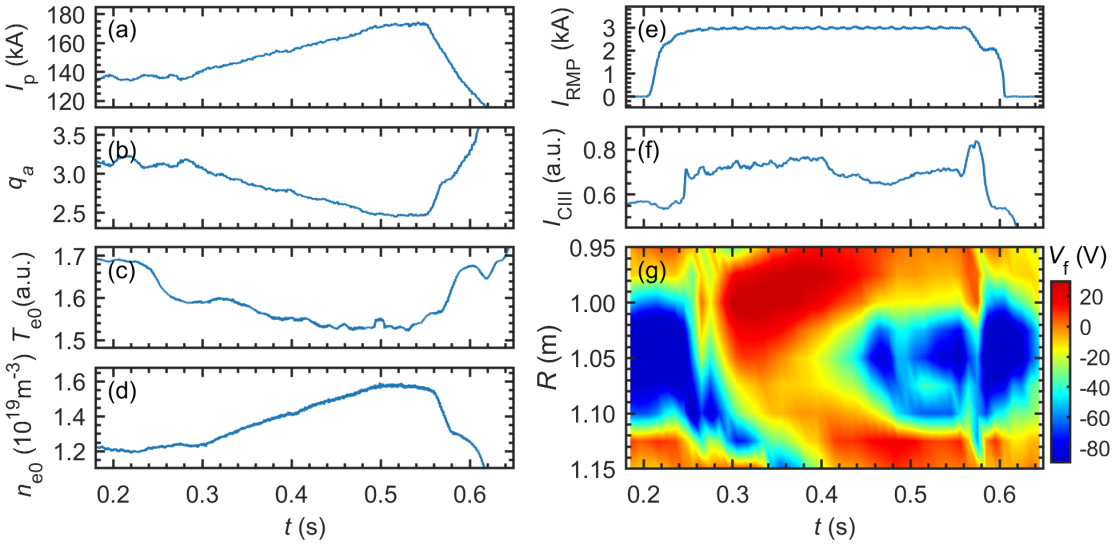

Figure 11*. Overview of main plasma parameters for the experiment discharge 1056902 on J-TEXT, including (a) the plasma current, (b) the edge safety factor, (c) the electron temperature, (d) the electron density, (e) the RMP coil current, (f) the CIII intensity near the plasma boundary, (g) the contour of the floating penitential measured by the divertor Langmuir probes.*

5.2 Stability of edge island

The operation of island divertor configuration is closely tied up with the stability of edge island. Once there is a change in the width and phase of the edge island, the island divertor configuration cannot operate stably, which can even lead to the deposition of heat-load outside the divertor targets. Therefore, the stability of edge island is of great concern in the experiment. A new type of edge island instability, a so called self-sustained divertor oscillation, was observed in J-TEXT (as shown in Fig. 12) during divertor experiments. Since a bifurcative oscillation of ~50 Hz is observed among the edge island width, the edge H_α intensity, and the edge electron temperature, the oscillation is regarded to be a sequential repetition of the magnetic field penetration-screening-transition and back-transition. The periodic collapses repeat several times until the edge islands are intersected by divertor target (corresponds to q_a = 3.1). As the edge islands are gradually opened, the amplitude of the oscillation decreases, and also the

properties of the oscillation change from burst-like (t = 0.31 ~ 0.38 s) to quasi-continuous (t = 0.38 ~ 0.42s). Thus, the divertor target structure is also significant for the stability of edge island. In addition, the divertor oscillation shows a correlated dependence on the plasma edge density. The detailed analyses and explanations are still to be investigated.

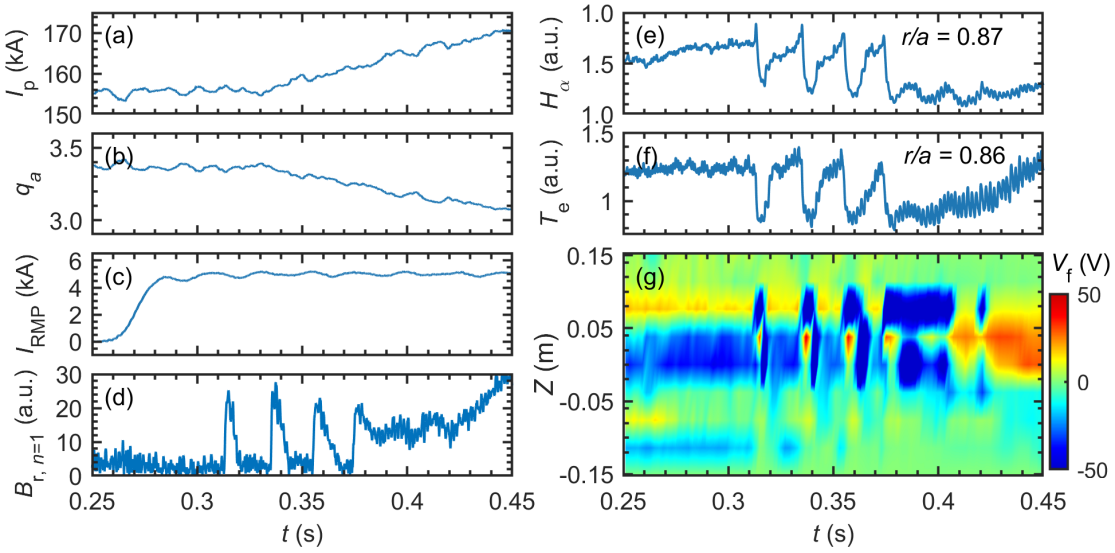

Figure 12. *Overview of main plasma parameters for the experiment discharge 1077700 on J-TEXT, including (a) the plasma current, (b) the edge safety factor, (c) the RMP coil current, (d) the radial magnetic field for the n = 1 part, (e) the H_α intensity, (f) the electron temperature and (g) the contour of the floating penitential measured by the divertor Langmuir probes.*

5.3 Impurity screening effects

The impurity accumulation at the central plasma is one of the burning issues for high-performance long-pulse plasma operation. Impurity control has become the focus of extensive attention in J-TEXT. During the application of the island divertor configuration, it was found that the m/n=3/1 edge island has an impurity screening effect, especially when the O-point of the island is near the low-field-side divertor target. By combining a methane injection experimental study and STRAHL impurity transport analysis, it was demonstrated that the variation of the impurity transport dominates the impurity screening effect. The impurity diffusion is enhanced with a significant increase in outward convection velocity at the edge region [58]. The interactions of the edge island and the divertor target contribute to the impurity screening effects with the dependence on the edge island width and phase. Therefore, a better impurity exhaust/screening could also be achieved by optimizing the edge magnetic topologies. In addition, the radial electric field, the plasma rotation and turbulence are considered to play an important role for impurity screening. The detailed impurity behaviors under the island divertor configuration will be studied with the foreseen application of 3D transport codes, such as EMC3-EIRENE. Moreover, combining of electric field, plasma rotation and turbulence into integrated scenario modeling is also an important topic for further studies.

5.4 3D divertor heat loads

For the island divertor configuration, longer field-line connection lengths at the SOL (in the magnitude of 10^2 - 10^3 m, much longer than the electron mean free path) could be obtained, which benefits heat-load spreading on the divertor target [59]. In order to investigate the effects of edge magnetic topology on divertor heat-load distribution, a two-dimensional infrared (IR) thermography camera system viewing the HFS divertor target from the LFS mid-plane window with a high spectral resolution of 0.5 mm has been established on J-TEXT. During the experiments in island divertor configuration, the surface temperature distributions on the divertor target could be obtained in real time. It was demonstrated that the divertor surface temperature distributions could be modified with the change of the edge magnetic topology. However, the leading edges on the existing divertor target seriously affect the measurement of heat-load. Thus, a new set of divertor target plates should be designed and constructed. Currently, an analysis program for extrapolating the divertor heat-load distribution from the divertor surface temperature is under development. Additionally, the heat-exhaust capabilities of the island divertor configuration will be investigated in the near future campaign.

5.5 Discussion & future challenges

The investigation of edge plasma physics relies heavily on appropriate diagnostics at the plasma boundary. In particular, in a tokamak equilibrium magnetic field configuration, the width of the edge island is generally narrow (w = 1 ~3 cm) due to the large magnetic shear, and therefore a high spatial resolution of the boundary diagnostics is greatly appreciated. In addition, owing to the 3D asymmetry of the island divertor configuration, measurements of edge plasma parameters need to be performed simultaneously at multiple (different poloidal and toroidal) locations during the experiment. Accordingly, the boundary diagnostics on J-TEXT are being gradually optimized and improved.

The key points of the island divertor research on J-TEXT are to demonstrate its performances of heat and particle exhaust. Moreover, it is worthwhile to explore how to realize stable detachment operation of the island divertor, which may rely on the synergy effects of the optimized magnetic topology, plasma transport and heat-load dissipation (through impurity seeding). Especially the core-edge integration to develop and demonstrate dissipative/detached divertor solutions for power and particle control, sufficient for extrapolation to high-performance long-pulse H-mode plasma conditions, is worth investigating.

6. Other new divertor concepts

The toroidal symmetric poloidal divertor configuration is usually modified to a 3D boundary by applying RMPs for the purpose of controlling ELMs [23, 60]. The RMP fields for ELM control are generally produced by in-vessel saddle coils, which may face great challenges in a future reactor, and have clear q_{95} windows.

Therefore, new approaches for generating RMP fields have to be proposed or tested. The non-axisymmetric (NA) helical currents induced by lower hybrid waves (LHW) in the SOL were observed to impact the magnetic topology profoundly and to strongly mitigate ELMs in EAST [23]. ELM control using NA-SOL currents induced by the NA biased divertor plates has been proposed and the RMP field driven by this technique is evaluated for ITER, and the predicted currents are sufficient to control ELMs in ITER [60].

These promising results motivate the experiments carried out on J-TEXT [61-63], which aim at verifying the ability of edge biasing driven NA-SOL currents to modify the boundary magnetic topology. The basic concept is to utilize the moveable electrode to apply a local biasing in the SOL of the J-TEXT plasma. Then the currents can be induced helically along the flux tubes towards the limiter or divertor plates, as illustrated in Fig. 13.

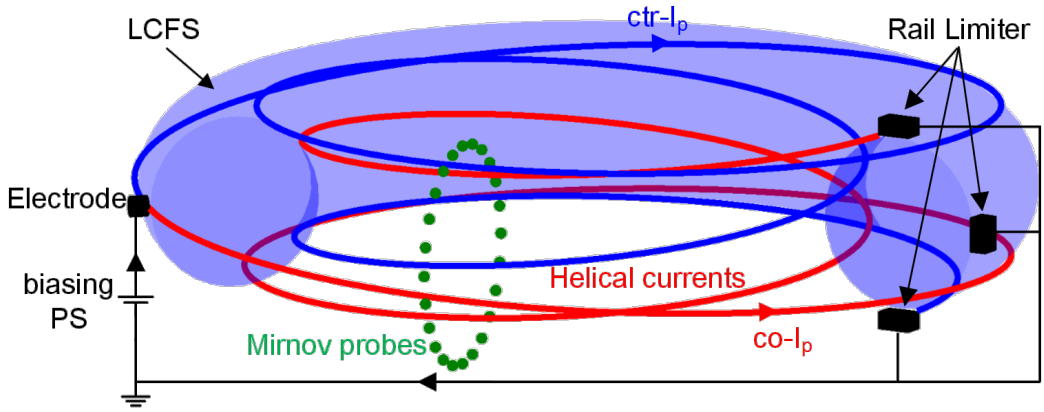

Figure 13 Schematic diagram for the SOL current driven by the biased electrode in the limiter plasma of J-TEXT.

As a first step, the experiments were carried out in the limiter configuration to study the basic features of the biasing driven SOL currents [61, 62]. By applying a modulated voltage to the electrode, the electrode current is modulated at the same frequency. Using the poloidal Mirnov probe arrays locating at two toroidal angles, the poloidal magnetic field is also measured to be modulated at the same frequency, and the amplitude (δB_θ) is shown in Fig. 14 with the total electrode current being 150 A. Clear peaks and valleys can be identified from the poloidal distribution of δB_θ, especially the peaks locates at different poloidal locations for the two arrays, indicating the toroidal NA feature of the magnetic perturbations (MPs). The squares in Figure 14 represent the calculated δB_θ obtained from a model with helical currents flowing in the flux tube of the electrode in either directions and decays to zero after a full poloidal turn. Most of the experimental features are captured by this simple model, proving that the biased electrode can induce helical current in the SOL and produce NA MPs.

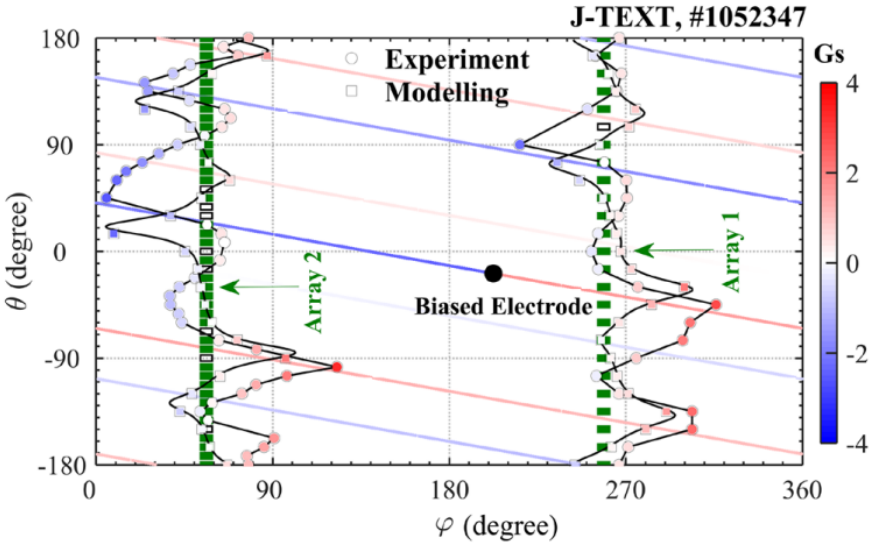

Figure 14 The comparison between measured δB_θ (circles) and modelled δB_θ (squares), showing the toroidal non-axisymmetric feature of the MPs generated by the biasing induced SOL currents. [61]

Further development of the model for biasing induced SOL currents improves the description and understanding of the experimental data [62, 64]. On one hand, by replacing the straight field line assumption with the toroidal geometry, the peaks/valleys of the modelled δB_θ lie exactly at the experimental ones [62]. Treating the electrode with finite size provides various flux tubes which then connect to various limiters, and more reasonable currents collected by the limiters can be calculated. On the other hand, using particle-in-cell simulations with simplified 2D geometric provides a physical understanding on the decay of the SOL current along the flux tube, i.e. the linear decay electron current is balanced by the ion cross field currents [64].

The SOL currents were then induced by electrode biasing in a poloidal divertor configuration on J-TEXT [63]. The NA feature of the corresponding MPs is also identified by the measurement from magnetic probe arrays. Modelling result shows that MPs with the amplitude of 14 G/kA for 4/1 component can be induced on the q_{95} surface (Figure 15). More importantly, the impact of NA-SOL currents on the boundary magnetic topology has been observed by the tangential visible CCD camera, as shown in Fig. 16. Figure 16 (a) displays the modelled Poincare plot near the X-point, where a clear lobe structure is observed above the upper divertor leg and it strikes the target at $Z \approx 0.04$ m. In the photo shown in Fig. 16 (b), the blue arrow indicates the upper divertor leg (or upper strike line) while the white arrow indicates the appearance of the lobe structure. This is clear evidence that the boundary magnetic topology can be modified by the NA-SOL currents induced via biasing. Since the current J-TEXT experiments use only a small electrode, the maximal amplitude of NA-SOL current is limited. Future experimental attempt with asymmetric divertor biasing [60] is attractive, and HL-2A seems to be prepared for the following challenge [65].

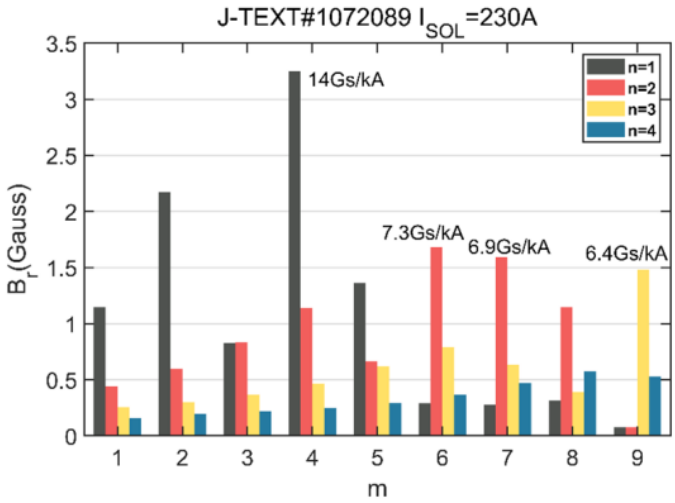

Figure 15 Radial magnetic field components obtained by the model on the q_{95} surface generated by the SOL current. [63]

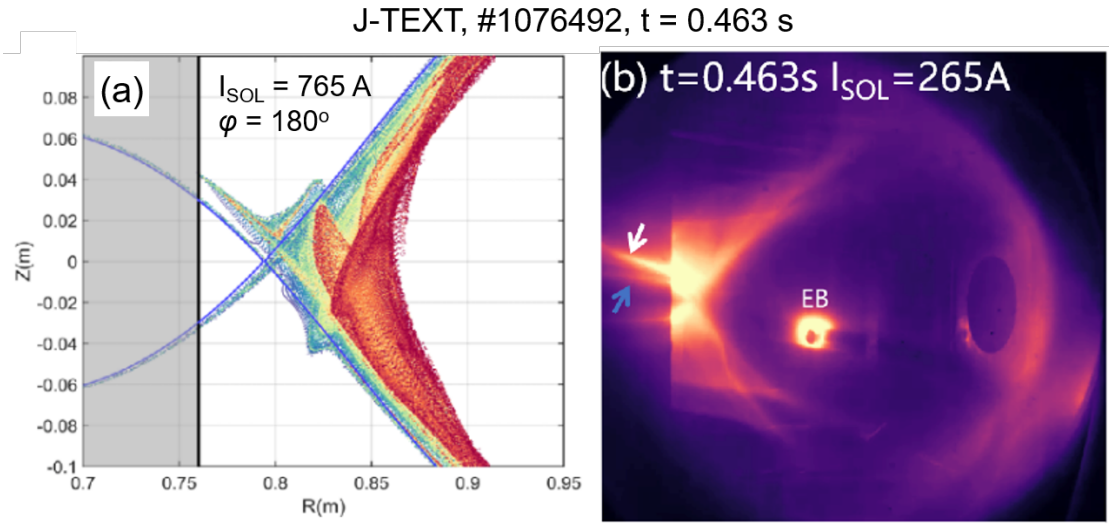

Figure 16 Impact of NA-SOL currents on the boundary magnetic topology in the poloidal divertor configuration. [63]

7. Summary

In summary, to support the study of advanced divertor configurations and their associated fundamental edge divertor plasma physics, the J-TEXT team has devoted considerable effort not only to the design of various new divertor configurations, but also to the development of edge plasma diagnostics and integrated modelling. Several important milestones have been achieved on J-TEXT in the last few years, which includes:

- First realization of the HFS-SN poloidal divertor plasma;
- Successful demonstration of using saddle coils to form island divertor plasmas in a tokamak device;
- First time use of bias electrodes to drive and actively control SOL current filaments to form 3D plasma boundaries.

Preliminary explorations of fundamental divertor plasma physics such as impurity screening/transport, density limit, up-down asymmetry of divertor loads, radiative divertor and detachment have been carried out on J-TEXT with those new divertor configurations. While the first experimental results are encouraging and interesting, further systematic studies and comparison with modelling results, especially on the synergy between 3D edge physics and plasma-wall interactions are still on-going.

Due to a limited heating capability, J-TEXT plasmas currently operate in low-confinement regime (L-mode). To extend the plasma operation domain and explore the coupling between new divertor configurations and high-performance core plasma, further upgrades of the ECRH heating system and development of new wall conditioning technology have been planned on J-TEXT.

8. Acknowledgements

This work is supported by the National MCF Energy R&D Program of China (Contract No. 2018YFE0309100, 2018YFE0310300), the National Key R&D Program of China (No. 2017YFE0302000) and the National Natural Science Foundation of China (Nos. 51821005).

References:

[1] M. Fujiwara *et al* 2001 Nucl. Fusion 41 1355

[2] B.N. Wan *et al* 2019 Nucl. Fusion 59 112003

[3] H.K. Park *et al* 2019 Nucl. Fusion 59 112020

[4] T. Klinger *et al* 2019 Nucl. Fusion 59 112004

[5] J. Bucalossi *et al* 2022 Nucl. Fusion 62 042007

[6] R. C. Wolf *et al* 2019 Phys. Plasmas 26, 082504

[7] C S Pitcher and P C Stangeby 1997 Plasma Phys. Control. Fusion 39 779

[8] T. Eich *et al* 2011 Phys. Rev. Lett. 107 215001

[9] M. Kobayashi *et al* 2013 Nucl. Fusion 53 093032

[10] Y. Feng *et al* 2005 Nucl. Fusion 45 89

[11] Finken K.H., Abdullaev S.S., Kaleck A. and Wolf G.H. 1999 Nucl. Fusion 39 637

[12] Y.Liang *et al* 2005 Phys. Rev. Lett. 94 105003

[13] L. Wang *et al* 2021 Nature Communications 12 1365

[14] N. Ohyabu *et al* 1994 Nucl. Fusion 34 387

[15] Y. Feng *et al* 2021 Nucl. Fusion 61 086012

[16] A. Bader *et al* 2017 Physics of Plasmas 24, 032506

[17] B. Labit *et al* 2017 Nuclear Materials and Energy 12 1015-1019

[18] E. Kolemen *et al* 2018 Nucl. Fusion 58 066007

[19] C. Zhang *et al* 2020 Fusion Engineering and Design 158 111678

[20] I. Katramados *et al* 2011 Fusion Engineering and Design 86 1595-1598

[20] T.E. Evans *et al* 2004 Phys. Rev. Lett. 92 235003

[21] Y. Liang *et al* 2007 Phys. Rev. Lett. 98 265004

[22] Y. Liang *et al* 2010 Phys. Rev. Lett. 105 065001

[23] Y. Liang *et al* 2013 Phys. Rev. Lett. 110 235002

[24] Y. Liang *et al* 2010 Nucl. Fusion 50 025013

[25] Y. Liang *et al* 2013 Nucl. Fusion 53 073036

[26] G. Zheng *et al* 2012 Chin. Phys. Lett. 29 105202

[27] G. Maddaluno *et al* 2017 Fusion Engineering and Design 122 341–348

[28] Y. Liang *et al* 2019 Nucl. Fusion 59 112016

[29] P. H. Edmonds et al 1988 Fusion technology (Proc. 15th Symp. Utrecht, 1988) vol. 1 North-Holland, Amsterdam p 342

[30] Y. Ding *et al* 2018 Plasma Sci. Technol. 20 125101

[31] X. Zhang *et al* 2022 Plasma Sci. Technol. 24 064007

[32] N. Wang *et al* 2022 Nucl. Fusion 62 042016

[33] Y. Wan *et al* 2017 Nucl. Fusion 57 102009

[34] Z. Chen *et al* 2012 Plasma Sci. Technol. 14 1041

[35] F. Li *et al* 2016 Rev. Sci. Instrum. 87 11D436

[36] Q. Yang *et al* 2022 Plasma Sci. Technol. 24 054005

[37] H. Liu *et al* 2016 Plasma Sci. Technol. 18 601

[38] H. Liu *et al* 2016 Rev. Sci. Instrum. 87 11D444

[39] J. Yang *et al* 2019 Plasma Sci. Technol. 21 105105

[40] M. Xia *et al* 2019 Fusion Eng. Des. 146 578

[41] Z. Cheng *et al* 2013 Rev. Sci. Instrum. 84 073508

[42] Z. Cheng *et al* 2014 Rev. Sci. Instrum. 85 11E423

[43] X. Zhang *et al* 2019 Fusion Eng. Des. 147 111241

[44] Y. Suzuki 2017 Plasma Phys. Control. Fusion **59** 054008

[45] Z. Wang *et al* 2021 Plasma Sci. Technol. 23 085104

[46] H. Wang *et al* 2021 Plasma Sci. Technol. 23 125103

[47] A. Knieps *et al* 2022 Plasma Phys. Control. Fusion 64 084001

[48] F. Wang *et al*, 2022 Nucl. Fusion 62 056021

[49] X. Xu *et al* 2022 Phys. Plasmas 29, 032510

[50] C. Han *et al* 2022 Fusion Engineering and Design 178 113099

[51] J. Huang *et al* 2021 Plasma and Fusion Research, 16 2403047

[52] H. Du *et al* 2016 Plasma Phys. Control. Fusion 58 085006

[53] V. Rozhansky *et al* 2012 Nucl. Fusion 52 103017

[54] N. Asakura *et al* 2004 Nucl. Fusion 44 503–12

[55] M. Jakubowski, et al 2021 Nucl. Fusion 61 106003

[56] Z. Huang *et al* Integrated design of new resonant magnetic perturbation coils on the J-TEXT tokamak, submitted to Plasma Science and Technology (2022).

[57] S. Zhou *et al 2019* Fusion Engineering and Design 146 902-905.

[58] X. Zhang *et al* 2021 Plasma Sci. Technol 23 125101

[59] S. Zhou *et al* 2022 Nuclear Fusion 62 106002.

[60] I. Joseph *et al* 2009 Phys. Plasmas 16 052510

[61] N.C. Wang *et al* 2019 Nucl. Fusion 59 096047

[62] S.H. Li *et al* 2021 Plasma Phys. Control. Fusion 63 115017

[63] S.H. Li *et al* 2022 Plasma Phys. Control. Fusion 64 075005

[64] H.X. Zhang *et al* 2020 Plasma Sci. Technol. 22 105102

[65] B.T. Cui et al 2021 Fusion Eng. Des. 173 112963